Low-frequency signature of magnetization nutation in nanomagnets

M. P. Adams [1,*] R. Bastardis [1,†] A. Michels [1,‡] and H. Kachkachi [2,§]

[1]*Department of Physics and Materials Science, University of Luxembourg, 162A avenue de la Faiencerie,*
L-1511 Luxembourg, Grand Duchy of Luxembourg

[2]*Université de Perpignan via Domitia, Lab. PROMES CNRS UPR8521, Rambla de la Thermodynamique,*
Tecnosud, 66100 Perpignan, France

In this work, we show that surface anisotropy in nanomagnets induces a nutational motion of their magnetization at various frequencies, the lowest of which can be described by the macrospin model whose dynamics is governed by an effective energy potential. We derive analytical expressions for the precession and nutation frequencies and amplitudes as functions of the size of the nanomagnet and its atomistic parameters, such as the exchange coupling and the onsite anisotropy. Our analytical model predicts a reduction of the precession frequency with increased surface anisotropy. We also simulate the dynamics of the corresponding atomistic many-spin system and compare the results with the effective model. We thereby show that the first nutation mode induced by the finite size and surface anisotropy occurs at a frequency that is four times larger than the precession frequency, thus lending itself to a relatively easy detection by standard experiments of magnetic resonance.

I. INTRODUCTION

Nutation is the well-known motion of a gyroscope described by classical mechanics; it develops whenever an external force tilts the rotation axis away from the direction of the gravity field since then the rotation axis no longer coincides with the direction of the angular momentum.

In the case of a magnetic material, magnetization nutation occurs whenever a time-dependent magnetic field (rf or microwave field) is present in the system. Accordingly, it has been demonstrated that there appears the fundamental effect of transient nutations in NMR [1], EPR [2], and optical resonance [3]. Spin nutation was first predicted in Josephson junctions [4] and was later developed using various approaches based on relativistic quantum mechanics, first principles [5,6], and electronic structure theory [7]. A more recent macroscopic approach [8] deals with the magnetization nutation by accounting for magnetic inertia through the addition of a second-order time derivative of the magnetization in the Landau-Lifshitz-Gilbert equation [9]. On the experimental side, evidence of the effects of nutation has been reported for thin films [10] in the THz regime. Indeed, magnetization nutation meets with a strong and expanding interest within the magnetism community owing to the real possibility of addressing and controlling the ultrafast magnetization dynamics, in view of potential practical applications in high-speed data processing and storage technologies based on magnetic materials. Considering the strong potential of achieving high

storage densities, this issue acquires still more enthusiasm for nanoscaled magnetic systems.

The dynamic behavior of nanomagnets (NM) requires a good understanding of the intricate interplay between different factors influencing the spin dynamics, such as finite-size, boundary, and surface effects. In particular, surface anisotropy emerges as a crucial parameter that can significantly influence the dynamics of nanomagnets as it affects the potential energy and thereby the relaxation rates [11]. Recently, it was shown [12] that spin misalignment, induced by surface effects, triggers nutational motion of the magnetization of a nanomagnet, with frequencies ranging from tens of GHz to THz, depending on various physical parameters, the predominant among them being the spin-spin exchange coupling and the onsite surface anisotropy. For example, in Refs. [13] it was shown that surface anisotropy in nanocubes triggers absorption modes of higher frequency than the ordinary uniform precessional motion with frequencies $f_p \sim 10$ GHz (conventional ferromagnetic resonance). More precisely, the authors of Ref. [12] observed a resonance at a frequency f_c that is four times f_p and another frequency f_n in the THz regime. While f_n is related to atomic spin fluctuations and their exchange coupling, the frequency f_c emerges from the cubic anisotropy induced by spin inhomogeneities at the surface of the nanomagnet [14]. As such, f_c corresponds to the nutational mode with the lowest frequency and should be more easily detected in resonance experiments on, e.g., arrays of nanomagnets with acute surface effects, such as platelets, pillars, spheres, or cubes.

In this work, we focus on the frequency f_c and derive its analytical expression using the effective macrospin model whose potential energy is a polynomial in the components of the net magnetic moment, with coefficients that are functions of the spin-spin exchange coupling and onsite anisotropy constants [14]. The results obtained using the effective model

---

*Contact author: michael.adams@uni.lu

†Contact author: roland.bastardis@univ-perp.fr

‡Contact author: andreas.michels@uni.lu

§Contact author: hamid.kachkachi@univ-perp.fr

are compared with those of numerical simulations for the corresponding many-spin nanomagnet. The effective model, thus validated, allows us to derive analytical expressions for the precession and nutation frequencies and the nutation amplitude and to study them in terms of the nanomagnet size and surface anisotropy.

Plan of the paper: We first define the many-spin and macrospin approaches and establish the connection between them. Then, we discuss the numerical results from both models for the time trajectories of the net magnetic moment. In particular, we discuss the results regarding the magnetization nutation and its dependence on the particle size and surface anisotropy. This study allows us to validate the effective model which is then used to derive the analytical expressions for the precession and nutation frequencies and amplitudes. From these expressions and further simulations, we draw the main conclusions of this work.

II. MODEL FOR THE MAGNETIZATION DYNAMICS

A. Many-spin approach (MSP)

In the many-spin problem (MSP) or many-spin approach, or still atomistic approach, the nanomagnet is regarded as a crystallite of a given shape and size, containing $\mathcal{N}$ atomic spins $\boldsymbol{S}_i = \mu_a \boldsymbol{s}_i$ located at the nodes of a given crystalline structure; μ_a denotes the atomic magnetic moment and $\boldsymbol{s}_i$ is a unit vector in the direction of $\boldsymbol{S}_i$. The magnetic state of such a system is studied with the help of the atomistic Hamiltonian [15–24]:

$$\mathcal{H} = \mathcal{H}_{\mathrm{exch}} + \mathcal{H}_Z + \mathcal{H}_A$$

$$= -\frac{1}{2} J \sum_{\langle i,j \rangle} \boldsymbol{s}_i \cdot \boldsymbol{s}_j - \mu_a \mathbf{B}_0 \cdot \sum_{i=1}^{\mathcal{N}} \boldsymbol{s}_i + \sum_{i=1}^{\mathcal{N}} \mathcal{H}_{A,i}, \quad (1)$$

where $\mathcal{H}_{\mathrm{exch}}$ is the nearest-neighbor (NN) exchange energy with $J > 0$, $\mathcal{H}_Z$ denotes the Zeeman energy with $\mathbf{B}_0 = \mu_0 \mathbf{H}_0$ being the homogeneous externally applied magnetic field, and $\mathcal{H}_A$ the magnetic anisotropy energy. For the core spins, we assume the anisotropy to be of uniaxial symmetry with constant K_c, while for surface spins we adopt the model proposed by Néel [25] with constant K_s. $\mathcal{H}_{A,i}$ is then given by

$$\mathcal{H}_{A,i} = \begin{cases} -K_c(\boldsymbol{s}_i \cdot \mathbf{e}_z)^2, & i \in \text{core} \\ +\frac{1}{2} K_s \sum_{j \in \mathrm{NN}} (\boldsymbol{s}_i \cdot \mathbf{u}_{ij})^2, & i \in \text{surface} \end{cases} \quad (2)$$

where the unit vectors $\mathbf{u}_{ij} = (\mathbf{r}_i - \mathbf{r}_j)/\|\mathbf{r}_i - \mathbf{r}_j\|$ connect the nearest-neighbor spins "i" and "j." All physical parameters are measured in units of energy per atom.

The (undamped) dynamics of the many-spin system is governed by the following Larmor equation:

$$\frac{d\boldsymbol{s}_i}{d\tau} = \boldsymbol{s}_i \times \boldsymbol{b}_{\mathrm{eff},i} \quad (3)$$

with the (normalized) local effective field $\boldsymbol{b}_{\mathrm{eff},i}$ acting on $\boldsymbol{s}_i$ being defined by $\boldsymbol{b}_{\mathrm{eff},i} = -\delta\mathcal{H}/\delta\boldsymbol{s}_i$; τ is the reduced time defined by

$$\tau \equiv \frac{t}{\tau_s}, \quad (4)$$

where $\tau_s = \mu_a/(\gamma J)$ is a characteristic time of the system's dynamics. By way of example, for cobalt $J = 8$ meV, leading

to $\tau_s = 70$ fs. Henceforth, we will only use the dimensionless time τ. Accordingly, the frequency $\omega = 2\pi f = 2\pi/T$ is measured in units of τ_s^{-1} and, as such, in the sequel $\nu \equiv \tau_s \omega$. Note that in these units, b_{eff} is equal to the effective field (in Tesla) multiplied by μ_a/J and is thus dimensionless.

To study the dynamics of this MSP, for arbitrary values of all physical parameters, one resorts to numerical methods for solving Eq. (3) using, for instance, the iterative routine based on the fourth-order Runge-Kutta scheme in combination with the projection step $\boldsymbol{s}_i^{\nu+1} = \boldsymbol{s}_i^{\mathrm{RK4}}/\|\boldsymbol{s}_i^{\mathrm{RK4}}\|$ to preserve the constraint $\|\boldsymbol{s}_i\| = 1$. The net magnetic moment $\boldsymbol{m}$ (unit vector) is then computed using

$$\boldsymbol{m} = \frac{\sum_i \boldsymbol{s}_i}{\|\sum_i \boldsymbol{s}_i\|}. \quad (5)$$

For the initial state of the system, we choose a coherent spin configuration along the orientation (θ_0, ϕ_0), i.e., $\boldsymbol{s}_i = (\sin\theta_0 \cos\phi_0, \sin\theta_0 \sin\phi_0, \cos\theta_0)$, for all $i = 1, \ldots, \mathcal{N}$.

Nutational motion was investigated in Ref. [12] using this MSP model and the results were compared with those of the macrospin model studied with the help of the augmented Landau-Lifshitz-Gilbert equation. In this work, our aim is to derive analytical expressions for the precession and nutation frequencies in terms of the atomistic parameters J, K_c, K_s and the size of the nanomagnet. For this purpose, we resort to the effective one-spin problem derived in Refs. [14] and compare the corresponding results with those obtained for the MSP in Ref. [12] in regard with the nutational motion.

B. Effective macrospin approach (EOSP)

The effective macrospin approach, or effective one-spin problem (EOSP), is obtained from the many-spin problem under certain conditions regarding the surface anisotropy, which should not be too strong with respect to the exchange coupling, and the particle size, which should not be too small (see Ref. [14] for details). The EOSP consists of the net magnetic moment (5) evolving in an effective energy potential given by

$$\mathcal{H}_{\mathrm{eff}} \simeq -k_2 m_z^2 + k_4 \sum_{\alpha=x,y,z} m_\alpha^4. \quad (6)$$

The values and signs of the (effective) coefficients k_2 and k_4 are functions of the atomistic parameters J, K_c, K_s, in addition to the size and shape of the nanomagnet and its underlying crystal lattice [14]. In the following, we will use the dimensionless constants defined by $k_c = K_c/J$ and $k_s = K_s/J$, so that k_2 and k_4 are dimensionless.

For a nanomagnet cut out of a simple cubic lattice, we have [14,26]

$$k_2 = k_c \frac{N_c}{\mathcal{N}}, \quad k_4 \simeq \begin{cases} \kappa \frac{k_s^2}{z}, & \text{sphere} \\ (1 - 0.7/\mathcal{N}^{1/3})^4 \frac{k_s^2}{z}, & \text{cube} \end{cases} \quad (7)$$

where $z = 6$ is the coordination number, κ represents a (dimensionless) surface integral, and N_c is the number of atoms in the core of the nanomagnet (with full coordination), while $\mathcal{N}$ is the total number of atoms (including both the core and surface). Note that κ was derived in Ref. [14] in the absence of core anisotropy. As shown in Ref. [27], in the presence of the latter, the spin misalignment caused by surface anisotropy
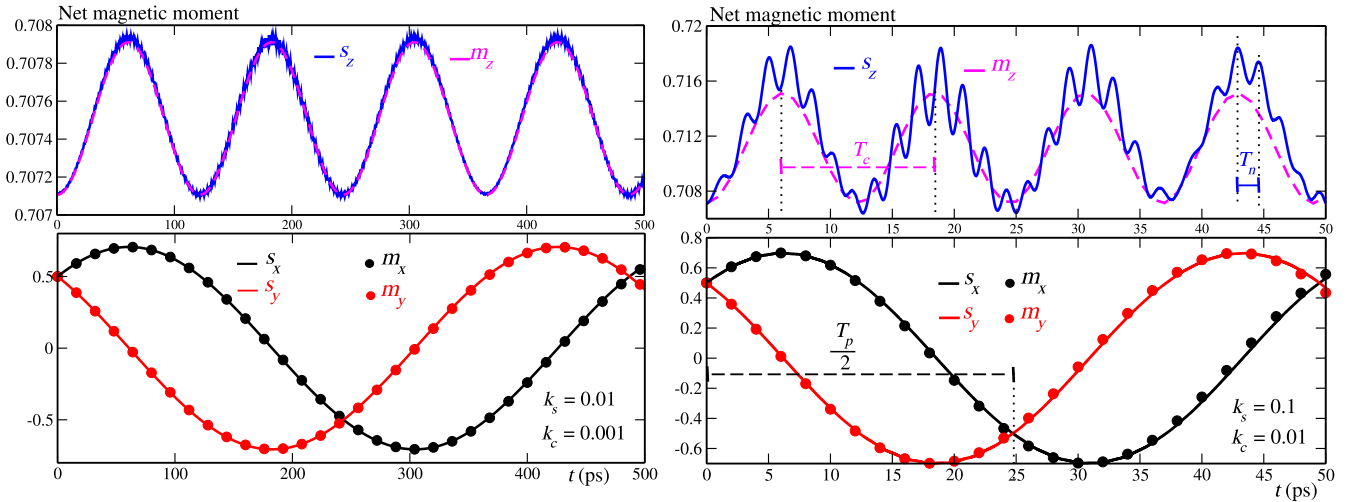
FIG. 1. Components of the net magnetic moment for both MSP (continued lines) and EOSP (dashed lines and symbols) for the spherical nanomagnet with a sc lattice and size $\mathcal{N} = 1088$. The constants k_c and k_s are indicated in the legend and the effective coefficients are given in Table I. On the right, T_p, T_c, T_n denote the periods corresponding to the respective frequencies f_p, f_c, f_n mentioned in the text.

does not propagate to the center of the nanomagnet; it is "fended off" by the uniaxial anisotropy in the core which tends to align all spins together. The result of this competition is that k_4 (or κ) is multiplied by the factor $N_c/\mathcal{N}$. Likewise, for both the cube and sphere, k_2 may be approximated [14] by the first expression in Eq. (7).

From the effective Hamiltonian in Eq. (6), we derive the following effective field that drives the dynamics of the magnetic moment $\boldsymbol{m}$

$$\boldsymbol{b}_{\text{eff}} = 2k_2 m_z \boldsymbol{e}_z - 4k_4\left(m_x^3 \boldsymbol{e}_x + m_y^3 \boldsymbol{e}_y + m_z^3 \boldsymbol{e}_z\right) \quad (8)$$

through the Larmor equation of motion for $\boldsymbol{m}$ as follows:

$$\frac{d\boldsymbol{m}}{d\tau} = \boldsymbol{m} \times \boldsymbol{b}_{\text{eff}}. \quad (9)$$

We would like to emphasize that the EOSP described here is not some variant of a single-domain macrospin model. Indeed, it is a macrospin model, but with coefficients that are functions of the atomistic physical parameters. In other terms, it has the advantage of being a "simple" macroscopic model which inherits (to some extent) the nanomagnet atomistic features, especially spin inhomogeneities.

Orders of magnitude of material parameters. Let us give a few orders of magnitude of the physical parameters that appear in the Hamiltonian (1) and Eqs. (7) and (8). Note that Eq. (1) is the energy per atom, obtained by dividing the total energy of the system by $\mathcal{N}$, the number of atoms in the NM. Hence, the physical parameters involved, namely, J, K, and $\mu_a(\mu_0 H)$, are measured in Joule per atom. For instance, the

anisotropy energy, which is often written as $\tilde{K}V$ where V is the volume of the NM and $\tilde{K}$ the density of anisotropy energy (in J/m^3), becomes $\tilde{K}V = \mathcal{N}v_0\tilde{K} \equiv \mathcal{N}K$. Similarly, the Zeeman contribution which usually reads as $\mu_0 HM$ is now rewritten as $\mathcal{N}\mu_a(\mu_0 H)$. For instance, for cobalt, the magnetic moment per atom is $\mu_a = n_0\mu_B$, with n_0 being the number of Bohr magnetons per atom ($n_0 \simeq 1.7$) and $\mu_B = 9.274 \times 10^{-24}$ J/T is the Bohr magneton. Hence, $\mu_a \simeq 1.58 \times 10^{-23}$ J/T. Next, the magnetocrystalline anisotropy constant is roughly $K_c \simeq 3 \times 10^{-24}$ J/atom, the surface anisotropy constant is around $K_s \simeq 5.22 \times 10^{-23}$ Joule/atom and the (bulk) exchange coupling is $J \simeq 8$ meV or 1.2834×10^{-21} J/atom. The lattice parameter is $a = 0.3554$ nm. As such, $k_c \equiv K_c/J \simeq 0.002\,34$ while $k_s \equiv K_s/J \simeq 0.04$. The latter value is within the range of values estimated by several experimental studies. Indeed, one may find $K_s/J \simeq 0.1$ for cobalt [28], $K_s/J \simeq 0.06$ for iron [29], and $K_s/J \simeq 0.04$ for maghemite particles [30]. In Ref. [14] we discussed the validity of the EOSP model for different lattice structures and NM shapes. In regards to this, the values of k_c and k_s used in our calculations are kept within the validity range of the EOSP model.

A final remark regarding the NM sizes we have considered in our calculations is in order. We want to emphasize that today, nanocubes (of iron or cobalt) are routinely investigated in experiments since their synthesis has become fairly well controlled [31–38]. For example, in Refs. [37,38], iron nanocubes of diameter in the range 5–25 nm are synthesized. Considering the size of an iron atom ($\sim$0.25 nm) and the interatomic distance ($\sim$0.3 nm) in a bcc lattice, the sizes used in our simulations, e.g., in Fig. 4, are well in the range achievable in experiments.

III. MAGNETIZATION NUTATION

A. MSP versus EOSP

In this section, we compare the dynamics of the net magnetic moment of different many-spin nanomagnets with that of the corresponding effective models for spheres [39],

TABLE I. Effective parameters used for the simulations on the nanospheres [from Eq. (7)].

$\mathcal{N} = 1088$ ($N_c = 706$)	k_2	k_4	ω_c(GHz)
$k_c = 0.001, k_s = 0.01$	6.5×10^{-4}	5.8×10^{-6}	51.5
$k_c = 0.01, k_s = 0.1$	6.5×10^{-3}	5.81×10^{-4}	515
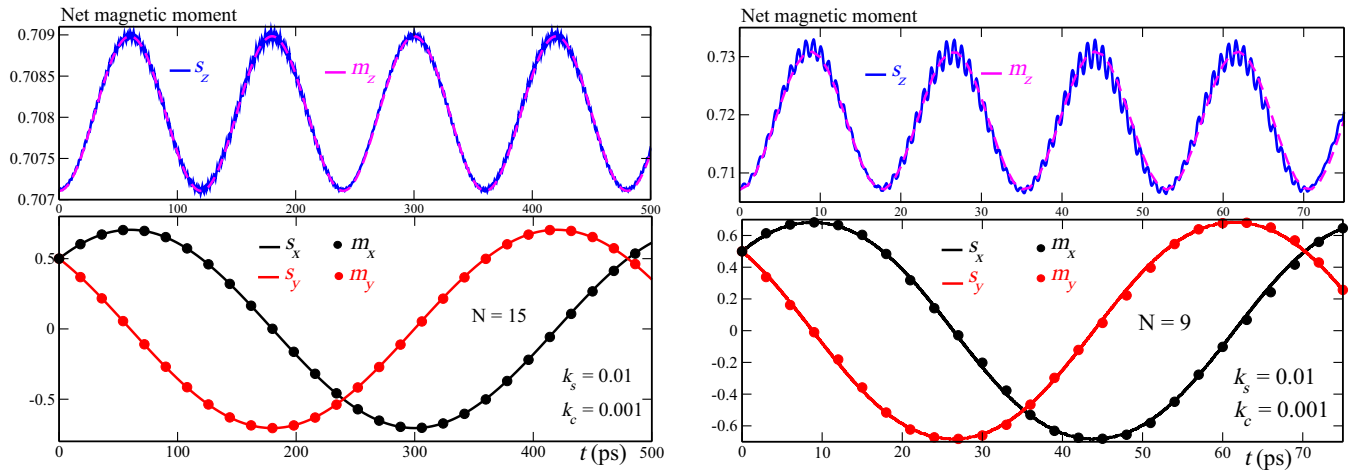
FIG. 2. Components of the net magnetic moment for both MSP (continued lines) and EOSP (dashed lines and symbols) for a cube-shaped nanomagnet with a sc lattice and sizes $\mathcal{N} = 15^3$ (left) and $\mathcal{N} = 9^3$ (right). The constants k_c and k_s are indicated in the legend and the effective coefficients are given in Table II.

cubes [13,31–36], and truncated octahedrons [14,40]. Before discussing the results in more detail, let us summarize the procedure followed for the comparison between the MSP and EOSP. For a given nanomagnet with a given size, shape, underlying lattice, and energy parameters (J, K_c, K_s), we solve the undamped Larmor equation (3) for all atomic spins s_i starting from the initial state (θ_0, ϕ_0) taken here to be ($\pi/4$, $\pi/4$). Then, we plot the components m_α (with $\alpha = x, y, z$) of the net magnetic moment (of the MSP) as functions of time.[1] Next, for a cube or a sphere with a simple cubic lattice, we use the expressions for k_2 and k_4 in Eqs. (7) to solve the Larmor equation (9) for the EOSP and obtain the components m_α as functions of time. For other shapes and/or lattice structures, such as the truncated octahedron or cubes with, e.g., body-centered-cubic (bcc) lattice (see Fig. 3), k_4 is obtained by fitting the MSP data. Note that in the case of an underlying bcc or fcc lattice, k_4 becomes negative [14].

The results of such a comparison confirm the following facts: the net magnetic moment of the many-spin nanomagnet exhibits three oscillation modes with different frequencies (see Fig. 1 right): the precession frequency f_p for the x, y components and the nutation frequencies f_c and f_n for the z component. The data in Figs. 1–3 are plotted as continued lines, in black and red for $s_{x,y}$ and in blue for s_z. The corresponding EOSP magnetic moment exhibits only two oscillation frequencies: the precession frequency f_p for $m_{x,y}$ (in red and black symbols) and the (smaller) nutation frequency f_c for m_z (in magenta). This result obtains in all cases of size, shape, and other physical parameters, as confirmed in Figs. 1–3. We see that as far as f_p and f_c are concerned, and this corresponds to the validity domain of the EOSP (i.e., relatively weak surface anisotropy), the dynamics of EOSP perfectly matches that of the MSP. However, the latter exhibits (in blue) an extra wiggling motion in the component

s_z (with frequency f_n) on top of a signal with frequency f_c. As mentioned in the Introduction and discussed in Ref. [12], the appearance of the frequency f_c is due to the quartic term in the Hamiltonian (6), which is a consequence of spin disorder induced by surface anisotropy in the EOSP regime; the coefficient of this term (k_4) is a function of K_s, as can be seen from Eq. (7). On the other hand, f_n is due to the fluctuations of the individual atomic spins with frequencies on the order of the exchange coupling J.

Further analysis of Figs. 1–3 reveals further useful information. First, the two frequencies f_p and f_c change with size, shape, and energy parameters. As the size decreases, the ratio $N_c/\mathcal{N}$ decreases, and the surface contribution to the overall energy increases [27]. Second, as the surface anisotropy constant K_s increases, the nutation frequency f_n is more clearly identified with an increasing amplitude. This effect is more clearly seen in Figs. 1 and 3 (plots on the right). However, the value of the frequency itself changes with the exchange coupling. Likewise, when going from the cube to the more rounded geometry of the sphere, through the truncated octahedron, we see that the nutational motion is progressively enhanced, and its amplitude increases.

B. Nutation frequency and amplitude: Analytical approach

From the previous section, we conclude that the effective model (EOSP) perfectly describes the dynamics of the many-spin nanomagnet as far as the validity conditions are met (i.e., small surface anisotropy). On the other hand, we have seen that, in addition to the nutation frequency f_c, the MSP exhibits another nutation mode with a much higher frequency f_n; the

---

[1]Note that in all plots we denote by s_α, $\alpha = x, y, z$, the Cartesian components of the net magnetic moment of the MSP and by m_α, $\alpha = x, y, z$, those of the magnetic moment of the EOSP.

TABLE II. Effective parameters used for the simulations on the nanocubes [from Eq. (7)].

$\mathcal{N}$	N_c	k_2	k_4	ω_c (GHz)
$729 = 9^3$	343	4.7×10^{-4}	12×10^{-6}	355
$3375 = 15^3$	2197	6.5×10^{-4}	13.8×10^{-6}	52
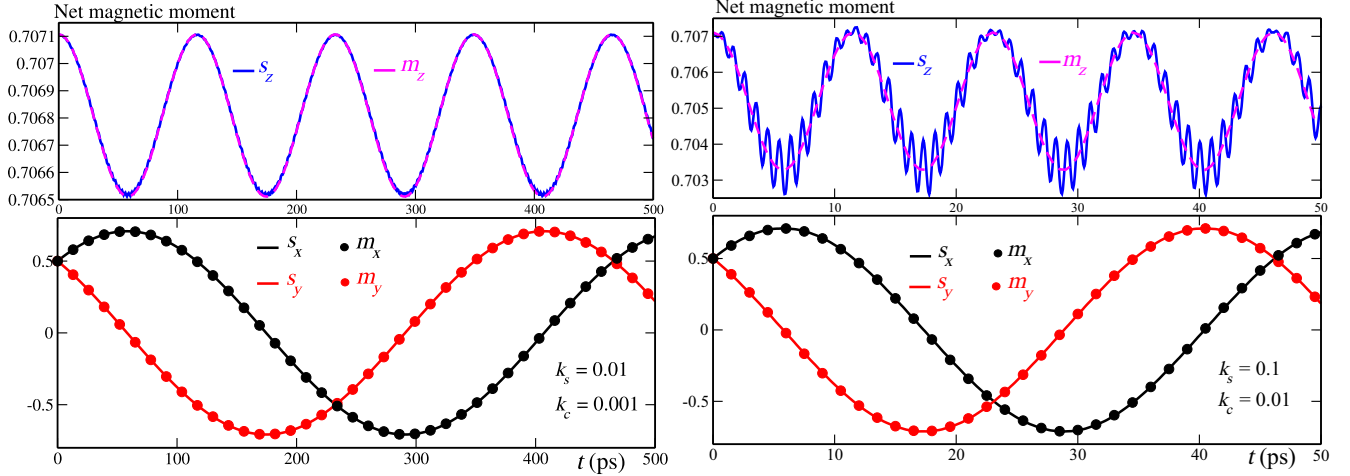
FIG. 3. Components of the net magnetic moment for both MSP (continued lines) and EOSP (dashed lines and symbols) for the truncated octahedron with fcc lattice and size $\mathcal{N} = 2075$. The constants k_c and k_s are indicated in the legend and the effective coefficients are given in Table III.

amplitude of this mode increases with the enhancement of surface effects, either through an increase of the anisotropy constant or that of the number of surface spins.

Now, with the macroscopic EOSP model at hand, we can derive analytical expressions for the frequency and amplitude of the precession and nutation modes and study their behavior in terms of surface anisotropy and size. Instead of the Cartesian components m_x, m_y, m_z of $\boldsymbol{m}$, it is more convenient

to parametrize the vector $\boldsymbol{m}$ using the spherical coordinates $\boldsymbol{q} = (\theta, \phi)$, with θ being the polar angle and ϕ the azimuth angle, i.e., $\boldsymbol{m}(\boldsymbol{q}) = (\sin\theta \, \cos\phi, \sin\theta \, \sin\phi, \cos\theta)$. Then, in this coordinate system, the Larmor equation (9) becomes

$$\frac{d\boldsymbol{q}}{d\tau} = \boldsymbol{b}'_{\text{eff}}(\boldsymbol{q}), \tag{10}$$

with the following effective driving field

$$\boldsymbol{b}'_{\text{eff}}(\boldsymbol{q}) = \begin{pmatrix} -k_4 \sin(4\phi) \sin^3\theta \\ -\cos\theta[2k_2 + (3 - 7\cos^2\theta)k_4] - k_4 \cos\theta \, \sin^2\theta \, \cos(4\phi) \end{pmatrix}. \tag{11}$$

Note that in Eq. (11), the appearance of trigonometric functions with the argument 4ϕ already hints to the fact that we should observe a mode with a frequency four times that of the "fundamental" mode, namely, the precession mode.

For the special case of $k_4 = 0$, the Larmor equation (10) with the driving field (11) has an exact analytical solution, where the polar angle $\theta(\tau) = \theta_0$ is time independent, while the azimuthal angle $\phi(\tau) = \phi_0 - (2k_2 \cos\theta_0)\tau$ is a linear function of time. Thus, the constant $\nu_{p,0} = 2k_2 \cos\theta_0$ is the precession frequency in the absence of k_4. For small but finite k_4, we expect the polar angle $\theta(\tau)$ to be an oscillating time-dependent function with a small amplitude, which can be treated as a small disturbance to the precessional motion. Thus, we approximate the driving field by a function of a precession-motion ansatz $\boldsymbol{q}_p(\tau)$, where the time dependence of θ is neglected, namely,

$$\frac{d\boldsymbol{q}}{d\tau} \simeq \boldsymbol{b}'_{\text{eff}}[\boldsymbol{q}_p(\tau)] \tag{12}$$

with

$$\boldsymbol{q}_p(\tau) = \begin{pmatrix} \theta_p(\tau) \\ \phi_p(\tau) \end{pmatrix} = \begin{pmatrix} \theta_0 \\ \phi_0 - \nu_p\tau \end{pmatrix}. \tag{13}$$

Here ν_p is the new precessional frequency, which is a function of k_2 and k_4. More explicitly, the approximate differential

equations for the angles θ and ϕ are

$$\frac{d\theta}{d\tau} \simeq -k_4 \sin^3\theta_0 \sin(4\phi_0 - 4\nu_p\tau),$$

$$\frac{d\phi}{d\tau} \simeq -\cos\theta_0[2k_2 + (3 - 7\cos^2\theta_0)k_4]$$
$$- k_4 \cos\theta_0 \sin^2\theta_0 \cos(4\phi_0 - 4\nu_p\tau). \tag{14}$$

Next, using a time integration in the form $\boldsymbol{q}_0 + \int_0^\tau \boldsymbol{b}'_{\text{eff}}[\boldsymbol{q}_p(\tau')]d\tau'$, with the initial condition $\boldsymbol{q}_0 = (\theta_0, \phi_0)$, we obtain the following approximate solution:

$$\theta(\tau) \simeq \theta_0 + \frac{k_4 \sin^3\theta_0}{4\nu_p}[\cos(4\phi_0) - \cos(4\phi_0 - 4\nu_p\tau)],$$

$$\phi(\tau) \simeq \phi_0 - \cos\theta_0[2k_2 + (3 - 7\cos^2\theta_0)k_4]\tau$$
$$+ \frac{k_4 \cos\theta_0 \sin^2\theta_0}{4\nu_p}[\sin(4\phi_0 - 4\nu_p\tau) - \sin(4\phi_0)], \tag{15}$$

TABLE III. Effective parameters used for the simulations on the truncated octahedrons obtained by a fitting procedure. Note that k_4 is negative for the fcc lattice [14].

$\mathcal{N} = 2075$	k_2	k_4	ω_c (GHz)
$k_c = 0.001, k_s = 0.01$	6.7×10^{-4}	-4.5×10^{-6}	54.6
$k_c = 0.01, k_s = 0.1$	6.7×10^{-3}	-2.9×10^{-4}	546
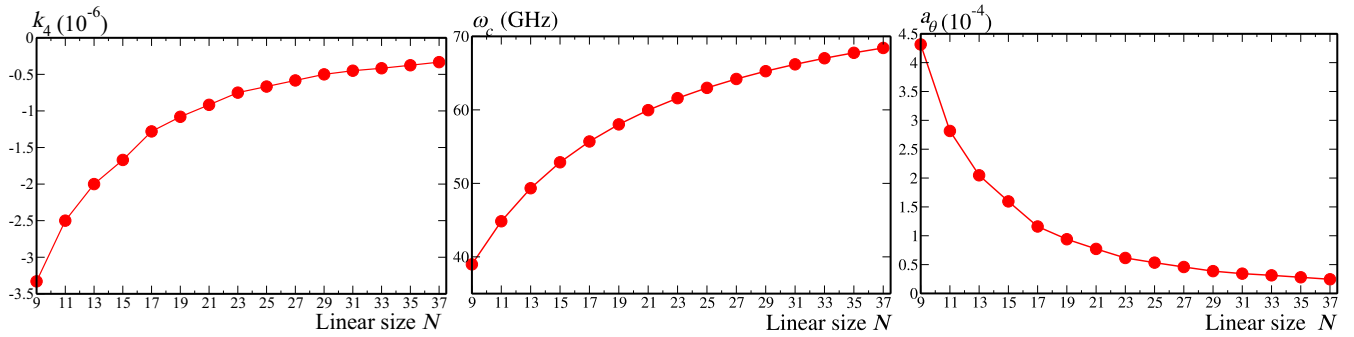
FIG. 4. EOSP parameter k_4, nutation frequency ω_c, and amplitude a_θ as a function of the linear size N of a bcc iron cube of size $N \times N \times N$ ($k_c = 0.001$ and $k_s = 0.01$). The parameters were obtained from a fit of the many-spin nanomagnet results to Eqs. (16)–(18). The full curves are guides to the eye.

which is, as expected, in the form of the precessional ansatz (13) plus additional terms in the form of oscillating functions. We find that the new precession and nutation frequencies are given by

$$\nu_p = \cos\theta_0 [2k_2 + (3 - 7\cos^2\theta_0)k_4],$$
$$\nu_c = 4\nu_p \tag{16}$$

with the corresponding amplitudes

$$a_\theta = \frac{k_4 \sin^3\theta_0}{4\nu_p},$$
$$a_\phi = \frac{k_4 \cos\theta_0 \sin^2\theta_0}{4\nu_p} = a_\theta \cot\theta_0. \tag{17}$$

In a more compact form, we may finally write

$$\theta(\tau) \simeq \theta_0 + a_\theta [\cos(4\phi_0) - \cos(4\phi_0 - 4\nu_p\tau)],$$
$$\phi(\tau) \simeq \phi_0 - \nu_p\tau + a_\phi [\sin(4\phi_0 - 4\nu_p\tau) - \sin(4\phi_0)]. \tag{18}$$

As mentioned earlier, in our calculations we start with all atomic spins s_i in the initial state $(\theta_0, \phi_0) = (\pi/4, \pi/4)$. In this case the solution (18) yields the time trajectories of the net magnetic moment ($a_\theta = a_\phi$):

$$\boldsymbol{q}(\tau) \simeq \begin{pmatrix} \frac{\pi}{4} \\ \frac{\pi}{4} - \nu_p\tau \end{pmatrix} + a_\theta \begin{pmatrix} -1 + \cos(4\nu_p\tau) \\ \sin(4\nu_p\tau) \end{pmatrix}. \tag{19}$$

The set of Eqs. (16)–(18) constitutes the original result of this work. Before discussing the conclusions we can draw from them, we summarize how they can be used in practice. Given a (many-spin) nanomagnet of a certain size and shape and a chosen set of energy parameters J, K_c, K_s, so that the spin configuration is not too much disordered, we can characterize the (modified) precession and the first nutation modes by their frequencies and amplitudes given by the corresponding effective macrospin model. If the nanomagnet is a nanocube or a nanosphere with an underlying simple-cubic lattice, the effective coefficients k_2 and k_4 are given by Eqs. (7). In the general case, one may fit the MSP curves $m_\alpha(\tau)$ to Eq. (18) and infer the quantities in Eqs. (16) and (17). In fact, once the constant k_4 is obtained, all the other quantities ($\nu_p, \nu_c, a_\theta, a_\phi$) can easily be derived. By way of illustration,

we have applied the latter procedure to the much-studied iron nanocubes [31,32,34,41,42] with an underlying bcc lattice. The results are shown in Fig. 4, where k_4, ω_c, and a_θ are plotted against the (linear) cube size N; the fit for k_4 yields $k_4 \simeq -12.5k_s^2/8(1 + N)^{5/3}$.

From Eqs. (16) and (17) and the numerical results in Fig. 4, we make the following observations:

(i) The frequencies ν_p and ν_c increase when the size increases but decreases with surface anisotropy, i.e., when K_s ($k_4 \propto k_s^2$) increases, for a small initial polar angle θ_0 (precession angle). For a relatively large angle θ_0 ($\gtrsim 49°$), the frequency becomes an increasing function of K_s (plot not shown).

(ii) The nutation frequency ν_c is four times the precession frequency ν_p, independently of the nanomagnet's size.

Regarding the amplitude, from Eqs. (17) we see that it increases with the surface anisotropy constant K_s, as already concluded from the results of the MSP simulations in Figs. 1–3. On the other hand, its behavior as a function of the size depends on the shape. In Fig. 4, we see that it is a decreasing function of N.

For a cube with simple-cubic lattice, $N_c/\mathcal{N} = (1 - 2/N)^3$ and thereby $a_\phi, a_\theta \sim 1/N$, which means that when the size increases, the nutation mode dies out. This has a very important implication. In general, any bulk or thin magnetic film presents an anisotropy energy that is an expansion in the components of its net magnetic moment, similar to the Hamiltonian in Eq. (6). However, the dynamics of a bulk magnetic material with such a Hamiltonian does not necessarily exhibit magnetic nutation. Here, we see that nanoscaled magnetic systems, such as nanocubes, do develop such a nutational motion at a frequency that should be observable in resonance experiments on arrays of such objects. For a sphere, using k_2 and k_4 from Eq. (7), Eqs. (17) imply that the amplitudes a_ϕ, a_θ do not depend on the size, as has also been confirmed by the MSP numerical simulations. For an arbitrary shape and/or lattice structure, it is not easy to derive simple formulas for the coefficients k_2, k_4. Nevertheless, as was discussed above, they may be obtained by fitting the dynamics of the net magnetic moment of the many-spin nanomagnet to Eqs. (18). This is what has been done for the bcc cubic nanomagnets, studied by experimental groups [13,31–36], and the results are shown in Fig. 4.

IV. CONCLUSION

We have shown that the magnetization of a nanoscaled magnetic material may exhibit nutational motion with frequencies in the GHz to THz range, the lowest of which is four times the precession frequency. We have provided analytical expressions for precession and nutation frequencies and the amplitude of the nutational oscillations as functions of the size of the nanomagnet and atomistic energy parameters, such as the spin-spin exchange coupling and the onsite surface and core magnetocrystalline anisotropies.

This has been possible owing to the correspondence we have firmly established between the many-spin approach and the effective macrospin approach, a correspondence that has been validated through numerical simulations of the dynamics of various nanomagnets (cubes, spheres, and truncated octahedrons) with different energy parameters and lattice structures. The results of these simulations have confirmed that the effective model recovers very well the dynamics of the many-spin nanomagnet in the low-frequency regime, when surface anisotropy is not too strong. In this regime, we observe the precession frequency f_p and the lowest nutation frequency f_c that is four times f_p and whose existence is related to the effective cubic anisotropy induced by spin inhomogeneities. The many-spin nanomagnet also exhibits a much higher frequency f_n that can be related to the spin-spin exchange coupling. Even the precession frequency f_p turns out to be affected by surface anisotropy, among other parameters. Within the effective macrospin model, we have demonstrated that the amplitude of the nutational motion is enhanced by surface anisotropy, but its behavior with the size depends on the shape of the nanomagnet.

All in all, in this work, we want to emphasize the fact that surface-induced magnetization nutation in nanoscaled magnets, such as nanocubes and nanospheres, already occurs at the lowest frequency which is four times the precession frequency, which itself is altered by spin misalignments. This low-frequency nutational oscillation lends itself to a detection and characterization using standard experimental techniques of magnetic resonance, such as the network analyzer with varying field and frequency, at low temperature. An array of well-separated platelets or nanocubes should provide adequate conditions for such measurements. Inelastic neutron spectroscopy [43] might also be able to resolve the predicted nutational spin dynamics in nanomagnets.

[1] H. C. Torrey, Transient nutations in nuclear magnetic resonance, Phys. Rev. **76**, 1059 (1949).

[2] N. C. Verma and R. W. Fessenden, Time resolved ESR spectroscopy. II. The behavior of H atom signals, J. Chem. Phys. **58**, 2501 (1973); P. W. Atkins, A. J. Dobbs, and K. A. McLauchlan, Transient nutations in electron spin resonance, Chem. Phys. Lett. **25**, 105 (1974); G. G. Fedoruk, Transient nutation EPR spectroscopy of condensed media (Review), J. Appl. Spectrosc. **69**, 161 (2002).

[3] G. B. Hocker and C. L. Tang, Observation of the optical transient nutation effect, Phys. Rev. Lett. **21**, 591 (1968).

[4] J.-X. Zhu and J. Fransson, Electric field control of spin dynamics in a magnetically active tunnel junction, J. Phys.: Condens. Matter **18**, 9929 (2006); J. Fransson and J.-X. Zhu, Spin dynamics in a tunnel junction between ferromagnets, New J. Phys. **10**, 013017 (2008); J. Fransson, Detection of spin reversal and nutations through current measurements, Nanotechnology **19**, 285714 (2008); Z. Nussinov, A. Shnirman, D. P. Arovas, A. V. Balatsky, and J. X. Zhu, Spin and spin-wave dynamics in Josephson junctions, Phys. Rev. B **71**, 214520 (2005); J.-X. Zhu, Z. Nussinov, A. Shnirman, and A. V. Balatsky, Novel spin dynamics in a Josephson junction, Phys. Rev. Lett. **92**, 107001 (2004).

[5] R. Mondal, M. Berritta, A. K. Nandy, and P. M. Oppeneer, Relativistic theory of magnetic inertia in ultrafast spin dynamics, Phys. Rev. B **96**, 024425 (2017).

[6] R. Mondal and P. M. Oppeneer, Relativistic theory of magnetic inertia in ultrafast spin dynamics, J. Phys.: Condens. Matter **32**, 455802 (2020).

[7] S. Bhattacharjee, L. Nordström, and J. Fransson, Atomistic spin dynamic method with both damping and moment of inertia effects included from first principles, Phys. Rev. Lett. **108**, 057204 (2012); M. Fähnle, D. Steiauf, and C. Illg, Generalized Gilbert equation including inertial damping: Derivation from an extended breathing Fermi surface model, Phys. Rev. B **84**, 172403 (2011); T. Kikuchi and G. Tatara, Spin dynamics with inertia in metallic ferromagnets, *ibid.* **92**, 184410 (2015); D. Thonig, O. Eriksson, and M. Pereiro, Magnetic moment of inertia within the torque-torque correlation model, Sci. Rep. **7**, 931 (2017); R. Cheng, X. Wu, and D. Xiao, Spin-mechanical inertia in antiferromagnets, Phys. Rev. B **96**, 054409 (2017).

[8] M.-C. Ciornei, J. M. Rubi, and J. E. Wegrowe, Magnetization dynamics in the inertial regime: Nutation predicted at short time scales, Phys. Rev. B **83**, 020410(R) (2011); E. Olive, Y. Lansac, and J. E. Wegrowe, Beyond ferromagnetic resonance: The inertial regime of the magnetization, Appl. Phys. Lett. **100**, 192407 (2012); J. E. Wegrowe and E. Olive The magnetic monopole and the separation between fast and slow magnetic degrees of freedom, J. Phys.: Condens. Matter **28**, 106001 (2016).

[9] L. D. Landau and E. M. Lifshitz, On the theory of dispersion of magnetic permeability in ferromagnetic bodies, Phys. Z. Sowjetunion **8**, 153 (1935); T. L. Gilbert, Formulation, foundations and applications of the phenomenological theory of ferromagnetism, Ph.D. thesis, Illinois Institute of Technology, Chicago (1956).

[10] Y. Li, A.-L. Barra, S. Auffret, U. Ebels, and W. E. Bailey, Inertial terms to magnetization dynamics in ferromagnetic thin

films, Phys. Rev. B **92**, 140413(R) (2015); K. Neeraj *et al.*, Inertial spin dynamics in ferromagnets, Nat. Phys. **17**, 245 (2021); V. Unikandanunni, R. Medapalli, M. Asa, E. Albisetti, D. Petti, R. Bertacco, E. E. Fullerton, and S. Bonetti, Inertial spin dynamics in epitaxial cobalt films, Phys. Rev. Lett. **129**, 237201 (2022); A. De, J. Schlegel, A. Lentfert, L. Scheuer, B. Stadtmüller1, Ph. Pirro, G. von Freymann, U. Nowak, and M. Aeschlimann, Nutation: Separating the spin from its magnetic moment, arXiv:2405.01334.

[11] P.-M. Déjardin, H. Kachkachi, and Yu. Kalmykov, Thermal and surface anisotropy effects on the magnetization reversal of a nanocluster, J. Phys. D **41**, 134004 (2008); F. Vernay, Z. Sabsabi, and H. Kachkachi, ac susceptibility of an assembly of nanomagnets: Combined effects of surface anisotropy and dipolar interactions, Phys. Rev. B **90**, 094416 (2014).

[12] D. Böttcher and J. Henk, Significance of nutation in magnetization dynamics of nanostructures, Phys. Rev. B **86**, 020404(R) (2012); R. Bastardis, F. Vernay, and H. Kachkachi, Magnetization nutation induced by surface effects in nanomagnets, *ibid.* **98**, 165444 (2018).

[13] R. Bastardis, F. Vernay, D. A. Garanin, and H. Kachkachi, Surface effects on ferromagnetic resonance in magnetic nanocubes, J. Phys.: Condens. Matter **29**, 025801 (2017).

[14] D. A. Garanin and H. Kachkachi, Surface contribution to the anisotropy of magnetic nanoparticles, Phys. Rev. Lett. **90**, 065504 (2003); H. Kachkachi and E. Bonet, Surface-induced cubic anisotropy in nanomagnets, Phys. Rev. B **73**, 224402 (2006); R. Yanes, O. Chubykalo-Fesenko, H. Kachkachi, D. A. Garanin, R. Evans, and R. W. Chantrell, Effective anisotropies and energy barriers of magnetic nanoparticles within the Néel's surface anisotropy, *ibid.* **76**, 064416 (2007); H. Kachkachi, Effects of spin non-collinearities in magnetic nanoparticles, J. Magn. Magn. Mater. **316**, 248 (2007).

[15] D. A. Dimitrov and G. M. Wysin, Effects of surface anisotropy on hysteresis in fine magnetic particles, Phys. Rev. B **50**, 3077 (1994).

[16] R. H. Kodama and A. E. Berkowitz, Atomic-scale magnetic modeling of oxide nanoparticles, Phys. Rev. B **59**, 6321 (1999).

[17] H. Kachkachi and D. A. Garanin, Boundary and finite-size effects in small magnetic systems, Phys. A (Amsterdam) **300**, 487 (2001).

[18] H. Kachkachi and D. A. Garanin, Spin-wave theory for finite classical magnets and superparamagnetic relation, Eur. Phys. J. B **22**, 291 (2001).

[19] O. Iglesias and A. Labarta, Finite-size and surface effects in maghemite nanoparticles: Monte Carlo simulations, Phys. Rev. B **63**, 184416 (2001).

[20] H. Kachkachi and M. Dimian, Hysteretic properties of a magnetic particle with strong surface anisotropy, Phys. Rev. B **66**, 174419 (2002).

[21] H. Kachkachi and D. A. Garanin, Magnetic nanoparticles as many-spin systems, in *Surface Effects in Magnetic Nanoparticles*, edited by D. Fiorani (Springer, Berlin, 2005), p. 75.

[22] N. Kazantseva, D. Hinzke, U. Nowak, R. W. Chantrell, U. Atxitia, and O. Chubykalo-Fesenko, Towards multiscale modeling of magnetic materials: Simulations of FePt, Phys. Rev. B **77**, 184428 (2008).

[23] M. P. Adams, A. Michels, and H. Kachkachi, Magnetic neutron scattering from spherical nanoparticles with néel surface

anisotropy: analytical treatment, J. Appl. Cryst. **55**, 1475 (2022).

[24] M. P. Adams, E. P. Sinaga, H. Kachkachi, and A. Michels, Signature of surface anisotropy in the spin-flip neutron scattering cross section of spherical nanoparticles: Atomistic simulations and analytical theory, Phys. Rev. B **109**, 024429 (2024).

[25] L. Néel, Anisotropie magnétique superficielle et surstructures d'orientation, J. Phys. Radium **15**, 225 (1954).

[26] D. A. Garanin, Effective anisotropy due to the surface of magnetic nanoparticles, Phys. Rev. B **98**, 054427 (2023).

[27] M. P. Adams, A. Michels, and H. Kachkachi, Spatial magnetization profile in spherical nanomagnets with surface anisotropy: Green's function approach, Phys. Scr. **98**, 105512 (2023).

[28] R. Skomski and J. M. D. Coey, *Permanent Magnetism, Studies in Condensed Matter Physics Vol. 1* (IOP Publishing, London, 1999).

[29] K. B. Urquhart, B. Heinrich, J. F. Cochran, A. S. Arrott, and K. Myrtle, Ferromagnetic resonance in ultrahigh vacuum of bcc Fe(001) films grown on Ag(001), J. Appl. Phys. **64**, 5334 (1988).

[30] R. Perzynski and Yu. L. Raikher, in *Surface Effects in Magnetic Nanoparticles*, edited by D. Fiorani (Springer, Berlin, 2005), p. 141.

[31] E. Snoeck, C. Gatel, L. M. Lacroix, T. Blon, S. Lachaize, J. Carrey, M. Respaud, and B. Chaudret, Magnetic configurations of 30 nm iron nanocubes studied by electron holography, Nano Lett. **8**, 4293 (2008).

[32] A. V. Trunova, R. Meckenstock, I. Barsukov, C. Hassel, O. Margeat, M. Spasova, J. Lindner, and M. Farle, Magnetic characterization of iron nanocubes, J. Appl. Phys. **104**, 093904 (2008).

[33] F. Jiang, C. Wang, Y. Fu, and R. Liu, Synthesis of iron oxide nanocubes via microwave-assisted solvolthermal method, J. Alloys Compd. **503**, L31 (2010).

[34] B. Mehdaoui, A. Meffre, L.-M. Lacroix, J. Carrey, S. Lachaize, M. Gougeon, M. Respaud, and B. Chaudret, Large specific absorption rates in the magnetic hyperthermia properties of metallic iron nanocubes, J. Magn. Magn. Mater. **322**, L49 (2010).

[35] F. Kronast, N. Friedenberger, K. Ollefs, S. Gliga, L. Tati-Bismaths, R. Thies, A. Ney, R. Weber, C. Hassel, F. M. Römer, A. V. Trunova, C. Wirtz, R. Hertel, H. A. Dürr, and M. Farle, Element-specific magnetic hysteresis of individual 18 nm Fe nanocubes, Nano Lett. **11**, 1710 (2011).

[36] C. O'Kelly, S. J. Jung, A. P. Bell, and J. J. Boland, Single crystal iron nanocube synthesis via the surface energy driven growth method, Nanotechnology **23**, 435604 (2012).

[37] Wetterskog *et al.*, Precise control over shape and size of iron oxide nanocrystals suitable for assembly into ordered particle arrays, Sci. Technol. Adv. Mater. **15**, 055010 (2014).

[38] S. Meftah, A.-T. Ngo, A. Shahmanesh, A. Courty, D. Kondo, F. Bedoui, and I. Lisiecki, Striking effect of the iron stearate purity on the shape and size of maghemite nanoparticles, Colloids Surf. A **680**, 132689 (2024).

[39] C. Salzemann, V. Russier, M. Pancaldi, P. Vavassori, A. Berger, and I. Lisiecki, High magnetic and super-structural uniformity in fcc supercrystalline films of co nanoparticles evidenced by moke, Colloids Surf. A **678**, 132473 (2023).

[40] M. Jamet, W. Wernsdorfer, C. Thirion, D. Mailly, V. Dupuis, P. Mélinon, and A. Pérez, Magnetic anisotropy of a single cobalt

nanocluster, Phys. Rev. Lett. **86**, 4676 (2001); M. Jamet, W. Wernsdorfer, C. Thirion, V. Dupuis, P. Mélinon, A. Pérez, and D. Mailly, Magnetic anisotropy in single clusters, Phys. Rev. B **69**, 024401 (2004).

[41] P. Tartaj, P. Morales, S. Veintemillas-Verdaguer, T. Gonzalez-Carreño, and C. Serna, The preparation of magnetic nanoparticles for applications in biomedicine, J. Phys. D: Appl. Phys. **36**, R182 (2003).

[42] M. Tran, Structural and magnetic properties of colloidal Fe-Pt and Fe cubic nanoparticles, Master's thesis, Institut National des Sciences Appliquees de Toulouse, Toulouse, (2006).

[43] Ch. Franz, S. Säubert, A. Wendl, F. X. Haslbeck, O. Soltwedel, J. K. Jochum, L. Spitz, J. Kindervater, A. Bauer, P. Böni, and Ch. Pfleiderer, MIEZE Neutron spin-echo spectroscopy of strongly correlated electron systems, J. Phys. Soc. Jpn. **88**, 081002 (2019).